Sound & Vibration 2026, 60(1), 3816. doi: https://doi.org/10.59400/sv3816

Article

Application of 3D-DIC in seismic response analysis of graphite core structures

Tianbao Lan[1,2,*], Zimin Zhan[1], Siqi Zhu[1]

[1] China Nuclear Power Engineering Co., Ltd., Beijing 100840, China

[2] School of Chemical Engineering and Technology, Tianjin University, Tianjin 300072, China

*** Corresponding author:** Tianbao Lan, lan.tianbao@163.com

CITATION

Lan T, Zhan Z, Zhu S. Application of 3D-DIC in seismic response analysis of graphite core structures. Sound & Vibration. 2026; 60(1): 3816. https://doi.org/10.59400/sv3816

ARTICLE INFO

Received: 8 December 2025
Revised: 21 January 2026
Accepted: 28 January 2026
Available online: 4 February 2026

Abstract: This study introduces and validates the application of the three-dimensional digital image correlation (3D-DIC) technique for the seismic assessment of graphite core structures in horizontal Micro-High-Temperature Gas-cooled Reactors (MHTGRs). Addressing a critical gap in conventional instrumentation, the non-contact 3D-DIC method was employed to capture the full-field vibrational response of individual graphite blocks within a loosely stacked core assembly under simulated seismic excitation. A full-scale reactor core model, comprising 31 discrete graphite blocks, was subjected to multi-axis seismic loading on a six-degree-of-freedom shaking table. The displacement-time histories and frequency-domain responses of each block were simultaneously measured using 3D-DIC and compared directly with data from traditional accelerometers. The 3D-DIC technique effectively eliminated the mass-loading and cable interference artifacts inherent in wired sensor arrays and captured the full field information of the graphite core structures. Comparative analysis in both time and frequency domains demonstrated amplitude correlations within ±10% between the two measurement methods. The results confirm that 3D-DIC provides a robust, high-fidelity, and non-invasive alternative for capturing complex, full-field structural dynamics in modular reactor cores. This work establishes a novel methodological framework for the seismic safety evaluation of advanced reactor designs and offers significant insights for enhancing structural health monitoring protocols in nuclear energy applications, thereby contributing to improved seismic resilience and operational safety of future high-temperature gas-cooled reactors.

Keywords: non-contact measurement; discrete core structure; vibration response; digital image correlation (DIC); high-temperature gas-cooled reactor (HTGR)

1. Introduction

Micro nuclear reactors represent an emerging technology offering flexible and diverse solutions for addressing energy challenges [1, 2]. The International Atomic Energy Agency (IAEA) defines micro nuclear reactors as nuclear power systems with electrical outputs below 10 MWe, featuring modular design and enhanced safety characteristics [3]. Currently, publicly disclosed micro nuclear reactors worldwide encompass various technologies, including high-temperature gas-cooled reactors (HTGRs), molten salt reactors, sodium-cooled fast reactors, lead-cooled fast reactors, heat pipe reactors, and light-water reactors. Among these technologies, HTGRs are particularly noted for their ability to operate at high temperatures and low pressures, achieving high thermal efficiency while maintaining inherent safety features. In HTGR designs, the graphite core structure serves as both the moderator

and primary structural component, making its integrity critical for ensuring the safe and stable operation of the entire reactor. However, the discrete nature of graphite block assemblies introduces unique structural challenges. Due to the nonlinear pin-key connections between the graphite bricks, the core structure exhibits complex nonlinear behavior under seismic loads [4]. For the validation of seismic design in such complex multi-body systems, extensive experimental data is required to support numerical simulations and ensure structural safety in seismic design. Therefore, it is critical to acquire reliable vibration data from graphite structures.

To address these seismic safety concerns, researchers worldwide have conducted numerous experimental studies on the seismic responses of various core structures, including the UK's Advanced Gas-cooled Reactor (AGR) [5], Japan's High-Temperature Test Reactor (HTTR) [6], Germany's pebble-bed High-Temperature Gas-cooled Reactor (HTGR) [7], and the commercially operational HTGR developed by Tsinghua University [8–11]. For instance, the HTR pebble-bed core underwent extensive testing with scaled models (including 1:2 side reflector, 1:6 cylindrical core configurations) to verify seismic stability [12, 13]. Similarly, the HTTR conducted tests on 1:2-scale single-column graphite models and sectional models [14–19]. In these experimental studies, accelerometers have traditionally been utilized to measure the structural acceleration responses of various models. However, this traditional measurement method faces challenges in installation when numerous measurement points are required, and the extensive cable networks may interfere with the structural response and compromise measurement accuracy. To address this limitation, Ni et al. adopted wireless accelerometers to reduce cable interference in discrete core vibration measurements [20]. In response to the extended lifespan of the graphite core structure in the UK's second-generation Advanced Gas-Cooled Reactor (AGR), researchers at the University of Bristol have systematically investigated its seismic response properties through a combination of quarter-scale physical modeling experiments and high-precision numerical simulations [21–23]. The core consists of multiple layers of polygonal graphite blocks interconnected by a system of keyways, which allows for limited oscillation while preventing tipping. A nonlinear finite element model with 35,000 degrees of freedom was developed, and an 8-ton physical model made from phenolic material (substituting for graphite) was configured with 3200 data channels. Measurements were conducted using wireless sensors. Lan et al. investigate the seismic performance of a horizontal graphite core model for gas-cooled microreactors, using a 1:1 partial planar model. Experiments combined accelerometers and digital image correlation to analyze responses under preloads of 15, 10, and 5 kN. Results show lower preload increases damping (up to 27%) and natural frequency (5 Hz vs. 4 Hz at 15 kN), due to enhanced lateral contact and internal friction. Seismic tests with 0.3 g ZPA confirmed structural integrity, with control rod channel displacements within 1 cm. The work highlights the nonlinear effect of preload and lateral gaps on dynamic behavior, providing key data for microreactor safety design [24]. Sai Sharath Parsi et al. employ a non-contact optical coordinate tracking system as the primary measurement method to characterize the seismic response of graphite block assemblies. A Polaris Vega XT optical tracker from Northern Digital Inc. (NDI)

was used. The study relied exclusively on advanced optical motion capture, rather than contact-based sensors like accelerometers, to obtain detailed kinematic data for validating numerical models of the core's seismic performance [25]. Mohtasham Khanahmadi presented a novel framework for structural health monitoring (SHM) based on modal dynamic flexibility [26]. It introduces an Irregularity Detection Index (IDI) to effectively localize single and multiple damages and identify their propagation paths in plates (composite and non-composite) and 1D elements (beams/columns). The method extracts damage-sensitive features from processed vibration signals. Validated through finite element models and calibrated experiments, the IDI demonstrates robustness against variations in damage severity, geometry, area, and noise, accurately highlighting damaged regions while ensuring localization in one area is unaffected by damage elsewhere. The framework provides a solid foundation for advanced SHM applications. Researchers used a vibration-based method for detecting interface debonding in concrete-filled steel tube (CFST) columns [27]. The proposed approach extracts damage-sensitive features by applying a 2D discrete wavelet transform to corrected modal signals. A key contribution is the development of the total normalized irregularity detection index (NIDI_T). Results from finite element models demonstrate that NIDI_T effectively identifies and localizes single and multiple debonding zones by accumulating irregularities in damaged areas. Critically, the method shows high diagnostic accuracy even for damage located at column ends and edges, addressing a significant challenge in structural health monitoring. The framework is validated for columns with different cross-sections and is robust to the choice of wavelet function. The above studies all demonstrate that non-contact measurement has certain advantages and applicability. While those approaches partially mitigate the cable interference issue, wireless accelerometers are significantly more expensive than conventional sensors, and their measurement accuracy was not quantitatively validated in their studies. These limitations highlight the need for advanced measurement techniques to provide comprehensive, non-contact, and precise measurements of complex multi-body structural systems.

In response to these technical challenges and measurement limitations, this study utilizes 3D-DIC to measure the response of a horizontally configured micro-HTGR featuring a discrete graphite block core. Through a comprehensive comparison of accelerometer measurements with 3D-DIC measurements in both time and frequency domains, this study evaluates the reliability and accuracy of the 3D-DIC technique for multi-component seismic monitoring applications. The findings provide critical validation for the application of 3D-DIC in seismic monitoring of discrete core structures and establish a foundation for advanced structural health monitoring approaches in modular reactor designs. This test can serve as a comparative reference for subsequent numerical analysis calculations and provide the displacement of the control rod orifice for control rod design.

2. Methodology

3D-DIC is a non-contact, full-field measurement technique for three-dimensional shape and deformation, which integrates binocular stereo vision and DIC matching

algorithms. This method first acquires the matching results of calculation points within the region of interest (ROI) from dual-camera images at different stages, along with the calibration parameters of the measurement system. It then combines these matching and calibration results for 3D reconstruction, ultimately determining the 3D positions of calculation points in the ROI at each stage to compute derived parameters such as displacement, velocity, and acceleration.

To address the requirements of multi-measurement-point synchronous tracking for discrete graphite brick cores, while balancing computational efficiency and accuracy, the image matching process employs a hierarchical strategy prioritizing integer-pixel search in the adjacent area. Points with a zero-mean normalized cross-correlation (ZNCC) below a preset threshold are marked as failure points, triggering an automatic switch to the GPU-accelerated SURF algorithm (a method that expands the matching range at the cost of longer computation time) to obtain initial values. Following sub-pixel precise matching via the DIC method, the 3D coordinates and displacements of calculation points across stages are calculated. Additionally, a neighborhood spatial averaging strategy is adopted to suppress noise and enhance displacement calculation accuracy, as the vibration of the graphite core is assumed to exhibit rigid-body motion. Specifically, for each manually selected calculation point, displacements of four neighboring measurement points are synchronously computed, and the mean value of these points is taken as the final displacement result. This spatial domain smoothing reduces the impact of random errors on single points, ensuring the stability of subsequent velocity and acceleration calculations.

Based on displacements, velocity and acceleration are derived using a point-wise curve fitting method, as the traditional difference method amplifies high-frequency noise, leading to cumulative errors and numerical distortion at boundaries or local extrema. For a given spatial point P, after obtaining its displacements at different stages, a fixed time window (7 stages in this experiment, comprising three preceding and three subsequent data points) is selected. A quadratic function of the displacement-time curve within this window is fitted using cubic B-spline interpolation combined with least squares optimization. The core impact of window size lies in balancing noise suppression and signal response: the selection of 7 as the time window (encompassing three points before and three points after the target moment) effectively filters out high-frequency random noise. An excessively large window may cause peak position lag; conversely, an overly small window risks insufficient data for fitting, failing to compensate for measurement fluctuations in discrete displacement time histories and thereby increasing variance in calculated peak velocity and acceleration. The smoothness of spline interpolation suppresses noise, while least squares fitting enhances the model's adaptability to discrete data. The choice of fitting function is directly related to the characteristics of the vibration signal: For the low-frequency rigid-body vibrations (below 50 Hz) of the graphite core, a quadratic function precisely matches the curvature changes in its displacement-time curve at an image acquisition frequency of 500 Hz. In contrast, low-order linear fitting tends to underestimate peak acceleration, while high-order polynomial fitting is prone to overfitting, leading to peak distortion. Finally, the first and second derivatives of the fitted function are numerically

computed as the point's velocity and acceleration at that moment. The data processing methods are summarized in **Figure 1**.

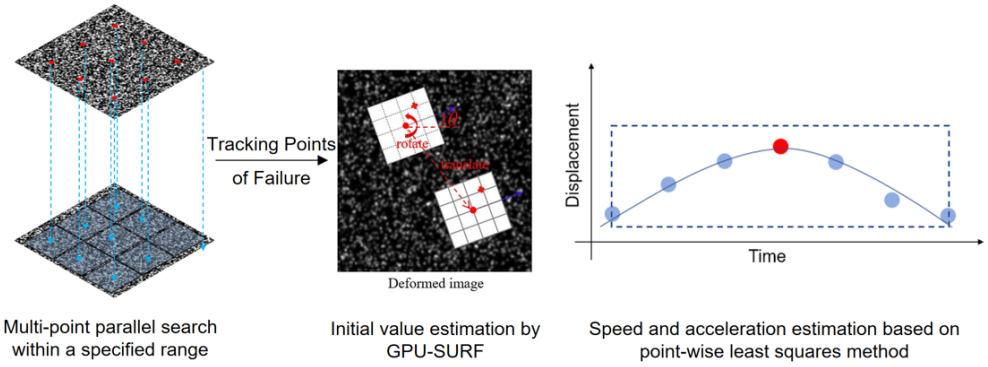

Figure 1. Schematic diagram of data processing.

2.1. Limitations

While 3D-DIC is a powerful non-contact measurement tool, its performance is fundamentally constrained by several physical and technical factors that must be carefully considered in experimental design, particularly for dynamic applications like seismic testing, such as lighting, sampling.

3D-DIC relies on consistent, high-contrast imaging of a speckle pattern. Inadequate, non-uniform, or fluctuating lighting leads to poor image correlation, increased noise, and data dropouts. This is especially challenging in large-scale, multi-camera setups.

High-speed events can cause motion blur with improper shutter speed, while highly reflective surfaces can create saturated pixels, both of which corrupt displacement data. DIC requires meticulous planning of stable, high-intensity, diffuse lighting systems (e.g., LED arrays) and careful control of ambient light.

The maximum achievable frame rate is inversely proportional to the camera's sensor resolution and the size of the field of view. Capturing high-frequency vibration (e.g., >1000 Hz) often requires sacrificing spatial resolution or measurement area.

DIC requires a priori estimation of the expected frequency range and selection of high-speed cameras capable of the necessary combination of resolution and frame rate, which increases cost and complexity. If the sampling frequency (frame rate) is not sufficiently higher than the highest frequency component of the structural response (typically >5–10 times the Nyquist rate), aliasing occurs, distorting the measured time-history data.

3D-DIC is an optical method requiring an unobstructed view from at least two calibrated cameras for every measured point on the specimen. In complex, three-dimensional structures (like a stack of graphite blocks), out-of-plane motion or the geometry of adjacent components can easily create occlusions, leading to permanent data loss in those regions.

DIC requires strategic, multi-camera placement from different angles to create overlapping fields of view and minimize "shadow" zones. Advanced multi-camera system calibration and data fusion are necessary, increasing setup complexity. During seismic tests, parts of the structure may move into the line of sight of others. This is

a critical challenge for monitoring multi-component assemblies where relative motion between parts is of interest.

In this experiment, these limitations necessitate a rigorous setup: high-speed cameras with sufficient resolution to track all 31 blocks, extremely stable and bright lighting to handle rapid motion, and a sophisticated multi-camera array to overcome occlusion in the loosely stacked assembly. The ±10% amplitude deviation reported likely reflects the practical noise floor imposed by these inherent constraints, even in a well-controlled laboratory environment. Acknowledging and quantifying these limitations is essential for correctly interpreting 3D-DIC data and validating it against other measurement techniques.

2.2. Accuracy verification

To verify the measurement accuracy of the DIC method, a cantilever beam vibration response test is conducted to assess the precision of the acceleration measurement algorithm. In this experiment, the cantilever beam is excited using a sinusoidal signal generator, while accelerometers are strategically placed on the beam to measure acceleration in the direction of deflection. Additionally, scattering features are incorporated on the accelerometers, and their acceleration is recorded using a non-contact, high-precision displacement measurement system. The accuracy of the acceleration measurements is validated by comparing the results obtained in the time domains.

2.3. Cantilever experimental verification

The experimental object is an aluminum variable-section beam with the specific dimensions illustrated in **Figure 2a**. The excitation device is a top-rod type excitation system, which includes an exciter (JZK-5 from Jiangsu Sunergy) and a signal generator (YE1311E from Jiangsu Sunergy). Before the experiment, the shaker was bolted to the profile support and secured 890 mm from the end of the cantilever beam using a connecting rod, as depicted in **Figure 2b**.

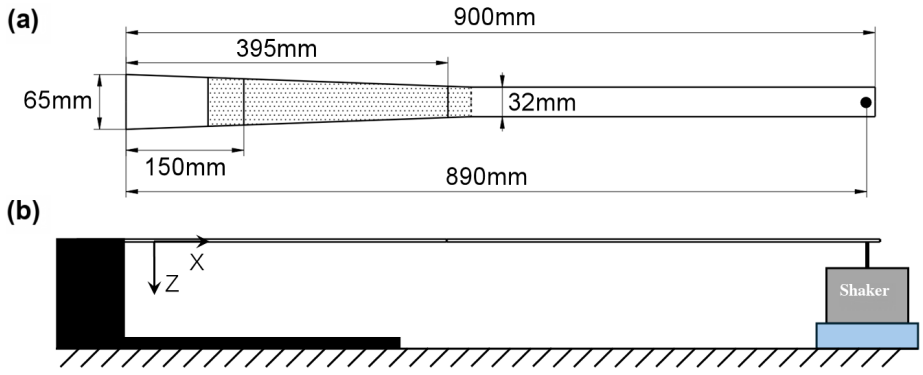

Figure 2. **(a)** Cantilever beam dimensions; **(b)** Shaker connection position.

After securing the position of the cantilever beam and the shaker, accelerometers were positioned at 50 mm intervals along the top surface to measure acceleration in the direction of beam deflection. Scattering spots, with an average diameter

of approximately 1.8 mm, were affixed to the sides of the accelerometers. The arrangement of the measurement points, along with the experimental and field images, is illustrated in **Figure 3**. Measurement points 0–4 correspond to accelerometers A, B, C, D, and E, respectively.

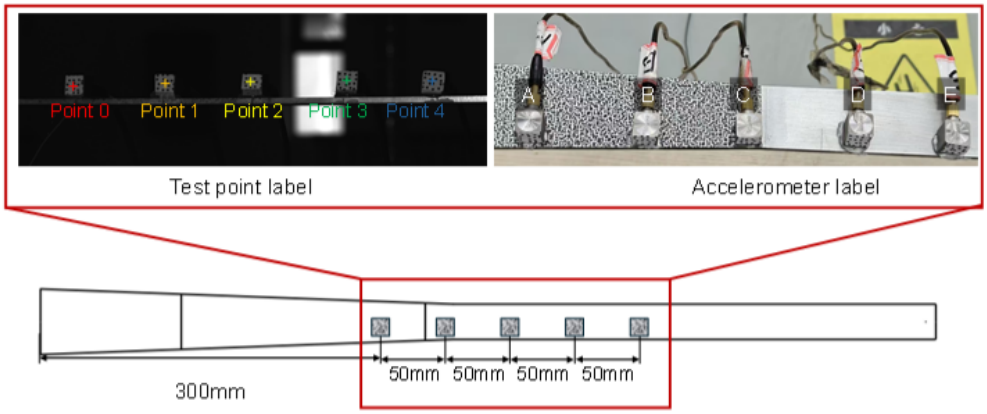

Figure 3. Position of the scattering spot, measurement point number, and accelerometer number.

During the experiment, the measurement system was positioned 1 m from the test piece. The spatial resolution of the system was approximately 0.167 mm per pixel, and the angle between the two cameras was about 25°. The size of the common field of view measured approximately 0.4 × 0.35 m. The dual high-speed cameras were synchronized using a trigger device, allowing the cameras to capture images at a constant frame rate of 500 Hz, which matched the accelerometer's rate. This frame rate is more than ten times the excitation frequencies of 20 Hz and 33 Hz. The experimental setup is illustrated in **Figure 4**.

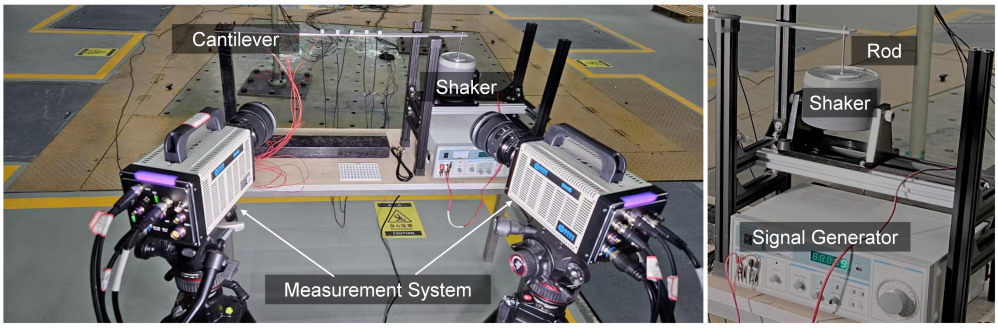

Figure 4. Experimental site.

2.4. Verification results

The time-domain comparison of acceleration from measurement point 0 to measurement point 3, along with their corresponding accelerometers, is plotted in **Figures 5** and **6** at an excitation frequency of 20 Hz and 33 Hz (with the initial time aligned).

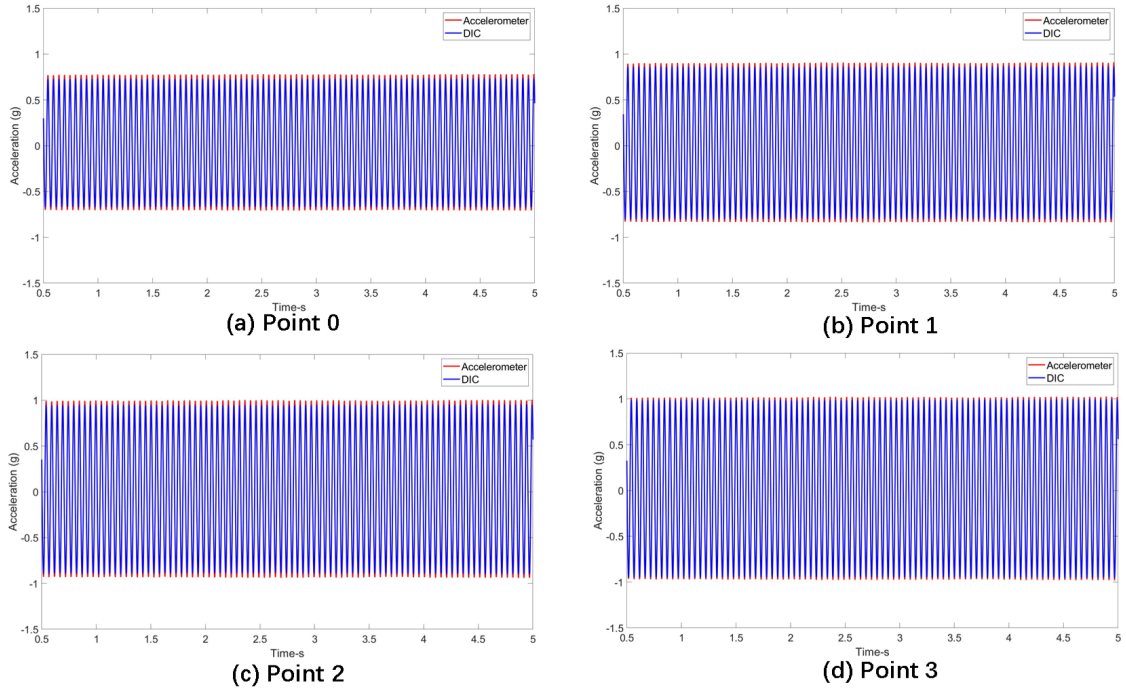

Figure 5. Comparison of acceleration time-domain results for 20 Hz excitation.

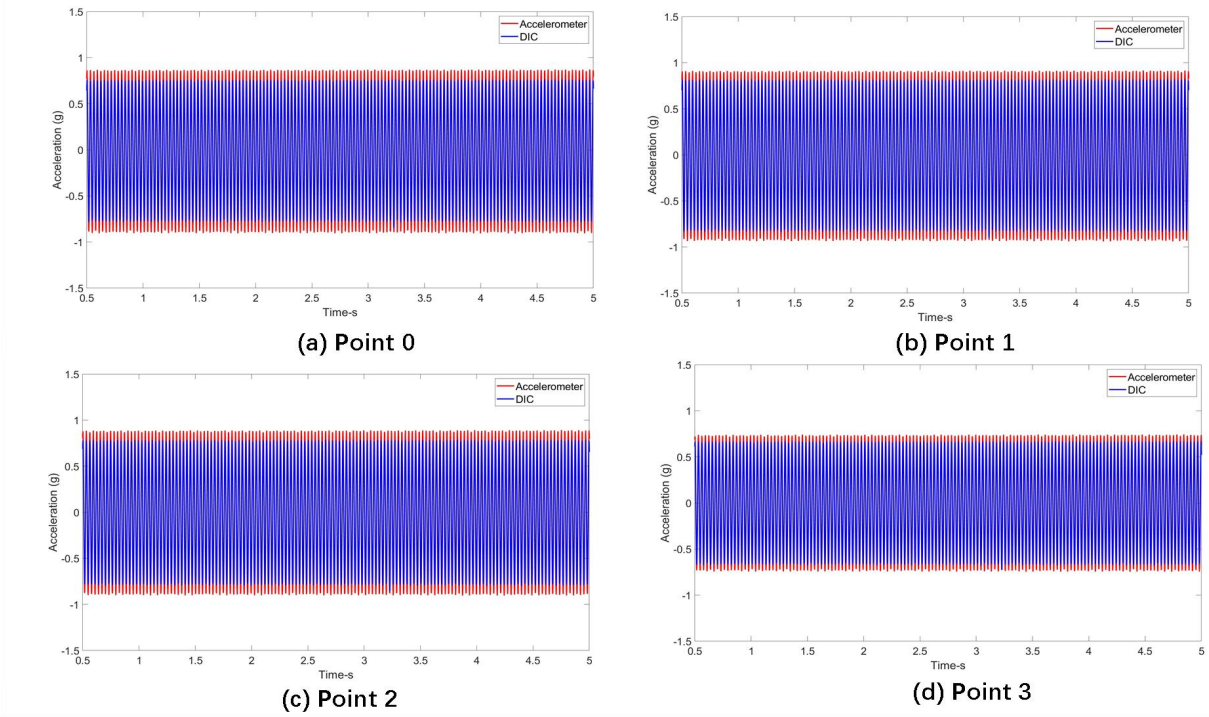

Figure 6. Comparison of acceleration time-domain results for 33 Hz excitation.

Non-contact measurements were consistently lower than those obtained from accelerometers; however, the total relative error remained within 10% shown in **Figure 7**. The error of the measuring system is therefore acceptable within 10% when the accelerometer results are set as the error reference.

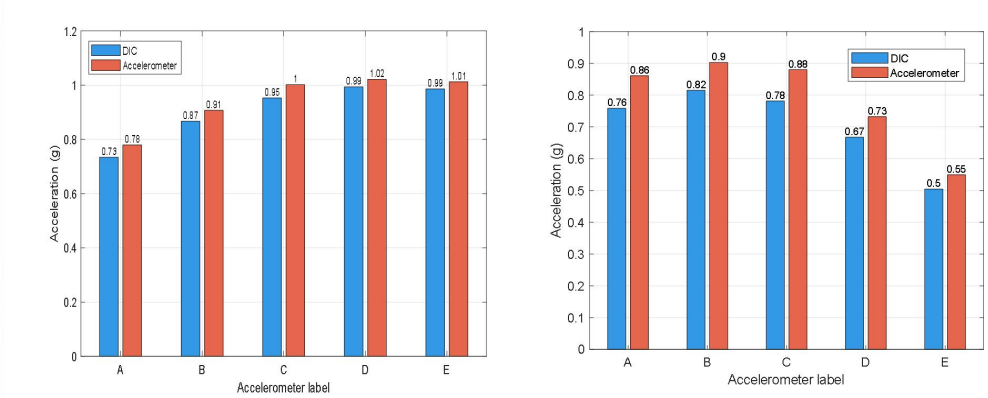

(a) Comparison at 20 Hz (b) Comparison at 33Hz

Figure 7. Comparison of peak acceleration at 20 Hz and 33 Hz.

The discrepancy between the measurement results obtained from the DIC method and those from the accelerometer can be attributed to two primary factors. First, when the cantilever beam vibrates, it experiences deflection. During this bending process, the accelerometer's measurement direction remains perpendicular to the cantilever beam, while the DIC method maintains its measurement direction in the initial orientation. As a result, the DIC method may only capture a portion of the maximum vibration, resulting in lower measurement values. Second, we employed a quadratic function to fit the velocity and acceleration data. However, the fitting accuracy of a quadratic function for peak values is inherently limited. Although increasing the sampling rate could improve this accuracy, excessively high sampling rates may adversely affect processing time. The current measurement accuracy is acceptable for engineering design. The measurement uncertainty will be considered in future designs.

3. Experiments

3.1. Specimen description

When conducting the seismic test design of the core, a substantial amount of test data is necessary to validate and support the numerical simulation results, ensuring the safety of the core structure. Given the nonlinear response of the core structure, a 1:1 scale model is employed to closely approximate the actual model, and a partial planar model test can be utilized. The model is composed of hexagonal graphite bricks and basic components with reflectors. For ease of processing, the graphite bricks used in the test model do not include airflow orifices.

The test object is a reactor core structure made of graphite materials. The graphite components are critical to the integrity of the core, and it is essential to investigate their performance under vibrational conditions to ensure safety. The core features a loosely stacked arrangement of internal graphite components, surrounded by an outer reflector that is secured with metal straps, shown in **Figure 8**. The working coordinate system for subsequent measurements is illustrated in **Figure 8**, with U representing the horizontal direction and V representing the vertical direction.

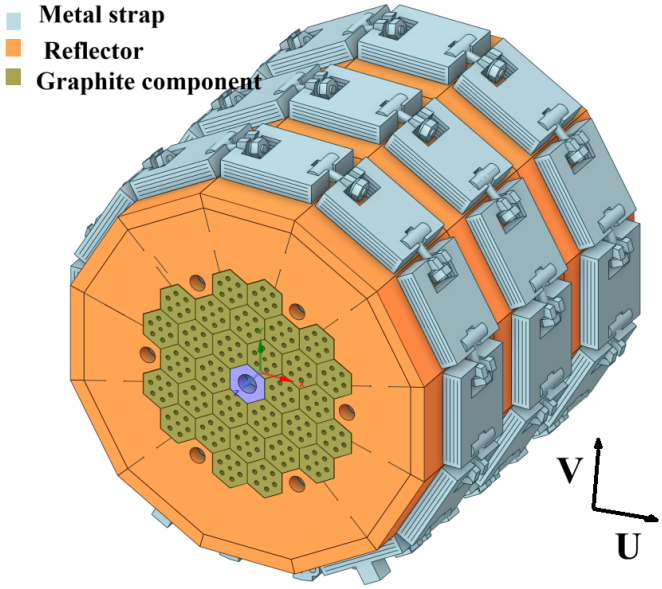

Figure 8. Horizontal layout of the core [28].

The model has both front and rear faces: the front face is speckled for imaging purposes, while accelerometers are installed on the rear (see **Figure 9**). According to the experimental environment, the field of view measures 3.17 m × 2.43 m, and the camera resolution is 2560 × 2016 pixels. Customized scattering stickers with an average diameter of 4.5 mm were created, consisting of adhesive-backed scattering stickers for tracking displacement, velocity, and acceleration. The adhesive-backed scattering stickers are hexagonal, with a side length of 120 mm, printed on adhesive-backed A4 paper and then cut to size. Non-contact measurement techniques can mitigate the motion interference caused by cables on the structure and allow for measuring the entire field.

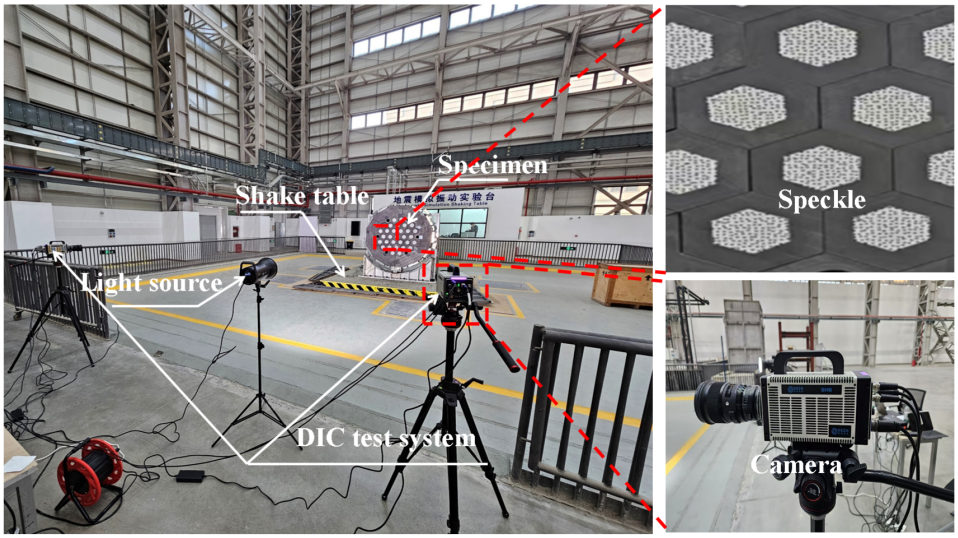

Figure 9. Test system and specimen on site.

3.2. Testing conditions

The specimen was mounted on a triaxial six-degree-of-freedom shaking table with a total weight of less than 8 t. To investigate the dynamic response of the graphite core in

service, this study employs a six-degree-of-freedom high-precision hydraulic shaking table to simulate its motion behavior under dynamic loads. The main performance parameters of the shaking table are presented in **Table 1**.

Table 1. Performance of the shake table.

Performance parameter	Value
Size of the table	3.2 m × 3.2 m
Maximum loads	10 t
Working frequency	0.1–100 Hz
Maximum acceleration	XYZ ≥ 2 g
Maximum velocity	XY ≥ 0.9 m/s, Z ≥ 1.1 m/s
Maximum displacement	XY ≥ 125 mm, Z ≥ 80 mm

The seismic design standard for the reactor core is based on withstanding no less than 0.3 times the spectra of RG 1.60. The input seismic acceleration time history (**Figure 10**) satisfied the design requirement of a zero-period acceleration (ZPA) of ≥0.3 g.

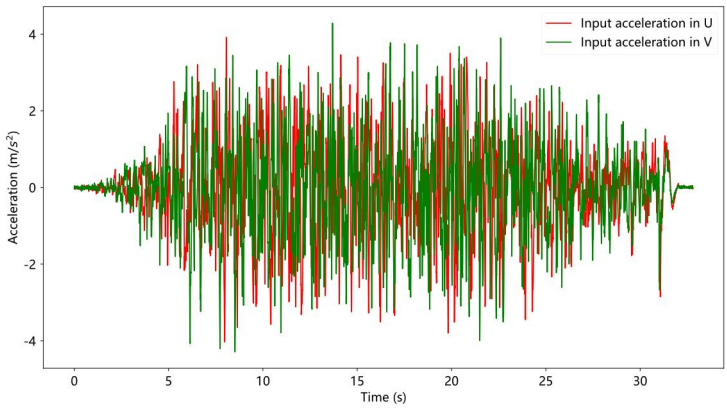

Figure 10. Input acceleration data for the model.

Two high-speed cameras, operating at 500 frames per second (fps) with a resolution of 2560 × 2016 pixels, were positioned 7 m from the specimen on vibration-isolated platforms, forming a 30° angle between them (see **Figure 9**). Custom hexagonal speckle patterns, with a side length of 120 mm and an average dot diameter of 4.5 mm, facilitated the tracking of displacement, velocity, and acceleration. The data from the cameras and accelerometers were synchronized at a frequency of 500 Hz.

3.3. Accelerometer configuration

Accelerometers are widely utilized for measuring structural acceleration, with a sampling frequency range of 0.1 Hz to 2000 Hz. However, limitations in cable length can restrict access to measurement points. In this study, the core consisted of 31 graphite bricks. Installing accelerometers on each brick would result in excessive cabling, which could interfere with the motion of the discrete structure. The use of a limited number of accelerometers is acknowledged as a constraint on spatial resolution for dynamic mode identification. However, they were strategically deployed to provide high-fidelity temporal benchmarks at critical points (e.g., the drive point and primary

antinodes). This design allows for a direct validation of the excitation profile and a point-wise comparison with time-differentiated DIC data, ensuring temporal accuracy. The comprehensive spatial analysis of mode shapes and strain distributions remains the exclusive domain of the full-field 3D-DIC measurements, with the accelerometer data serving as anchored validation points within the broader displacement field. To address this issue, lightweight uniaxial accelerometers (weighing less than 30 g) were deployed. For validation purposes, accelerometers were installed on specific graphite components (Accel-2, Accel-3, Accel-A to E). Accel-2 and Accel-3 were biaxial, measuring in the horizontal (U) and vertical (V) directions, while Accel-A to E were uniaxial, measuring only in the horizontal (U) direction. The measurement coordinates are illustrated in **Figure 11**.

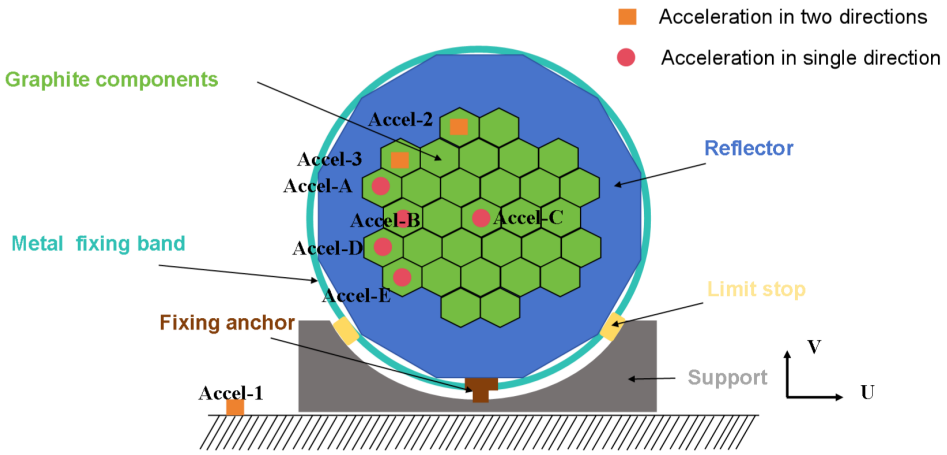

Figure 11. Accelerometer installation points on the backside.

4. Results

4.1. Time-domain results

Time-domain acceleration comparisons are shown in **Figure 12**. **Figure 12e,f** displays the resultant acceleration (Equation (1)) for Accel-2 and Accel-3, calculated as:

$$Acc = \sqrt{Acc_U{}^2 + Acc_V{}^2} \tag{1}$$

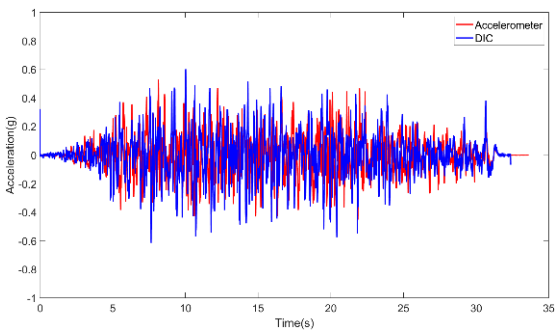

(a) Comparison of acceleration U direction at point 2.

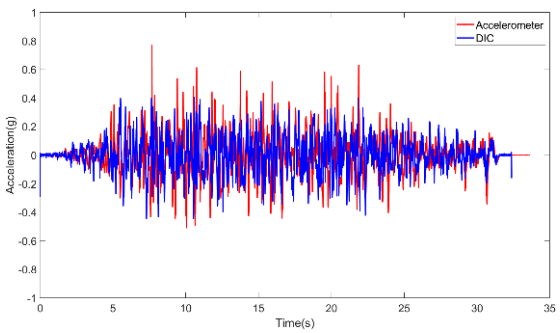

(b) Comparison of acceleration V direction at point 2.

Figure 12. *Cont.*

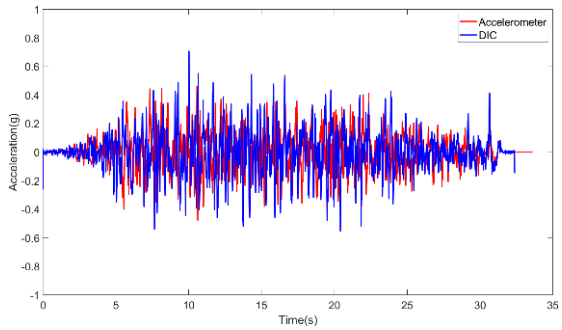

(c) Comparison of acceleration U direction at point 3.

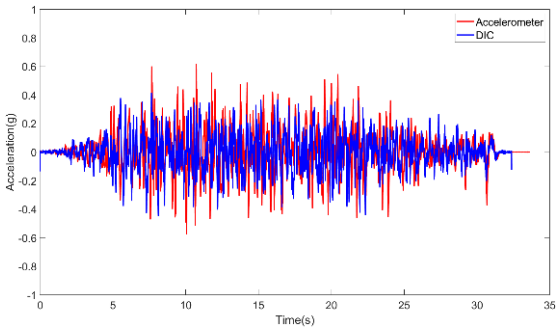

(d) Comparison of acceleration V direction at point 3.

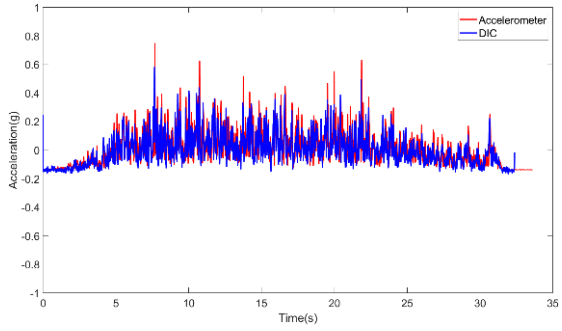

(e) Comparison of acceleration UV synthetic direction at point 2.

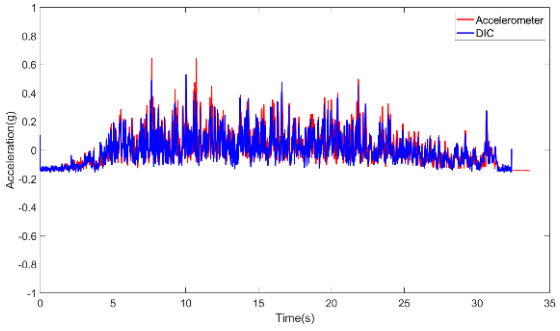

(f) Comparison of acceleration UV synthetic direction at point 3.

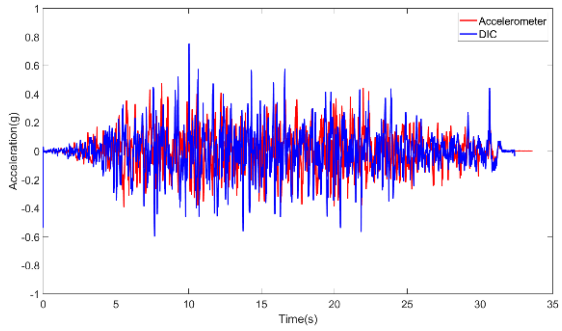

(g) Comparison of acceleration U direction at point A.

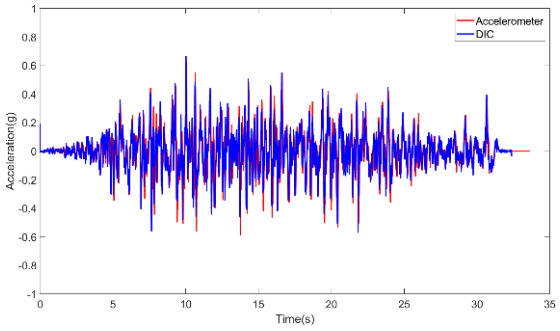

(h) Comparison of acceleration U direction at point B.

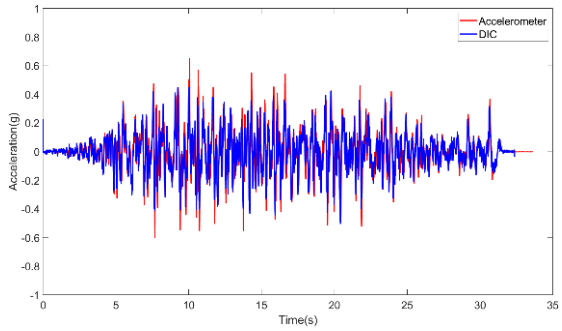

(i) Comparison of acceleration U direction at point C.

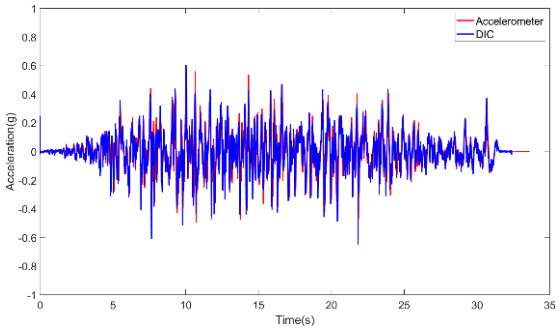

(j) Comparison of acceleration U direction at point D.

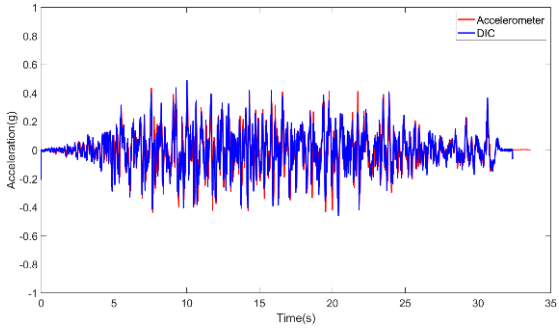

(k) Comparison of acceleration U direction at point E.

Figure 12. Time domain comparison between DIC measurements and accelerometer results.

It can also be observed from **Figure 12** that the acceleration at measurement points 2 and 3 is significantly greater than the acceleration response at measurement point E. This indicates that the higher the position of the graphite assembly, the larger the acceleration response.

4.2. Frequency domain results

The Fourier transform of the above time domain results yields the frequency response curve shown in **Figure 13**.

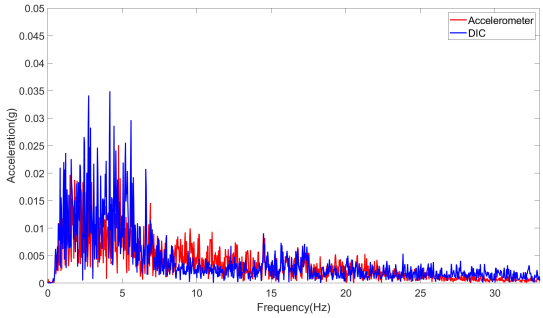

(a) Comparison of acceleration U direction at point 2.

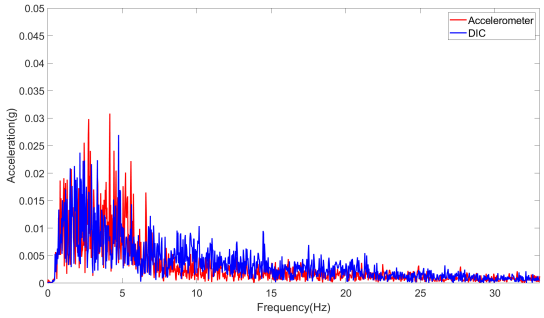

(b) Comparison of acceleration V direction at point 2.

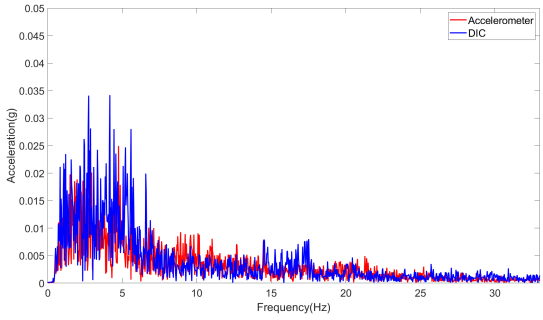

(c) Comparison of acceleration U direction at point 3.

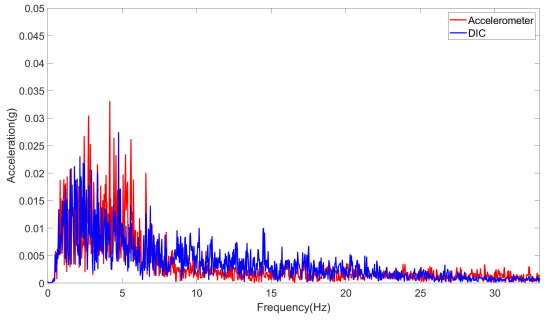

(d) Comparison of acceleration V direction at point 3.

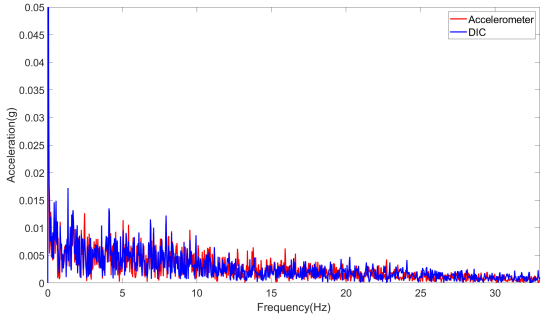

(e) Comparison of acceleration UV synthetic direction at point 2.

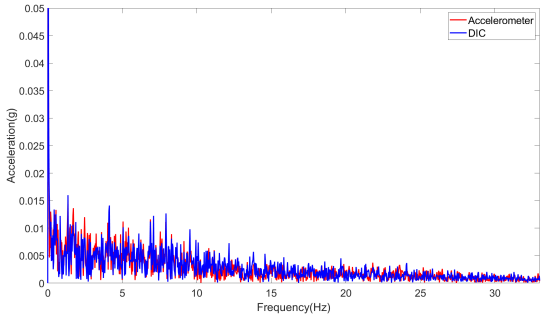

(f) Comparison of acceleration UV synthetic direction at point 3.

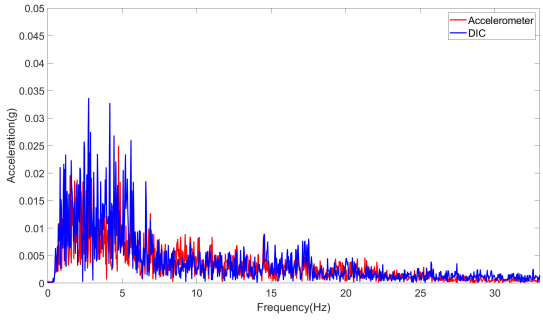

(g) Comparison of acceleration U direction at point A.

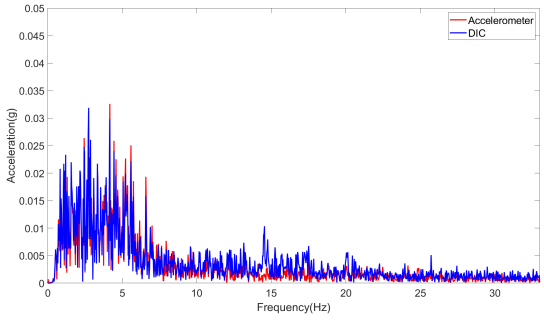

(h) Comparison of acceleration U direction at point B.

Figure 13. *Cont.*

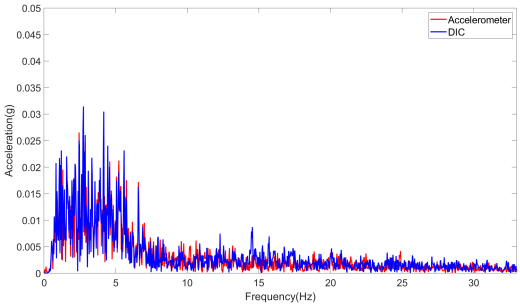

(i) Comparison of acceleration U direction at point C.

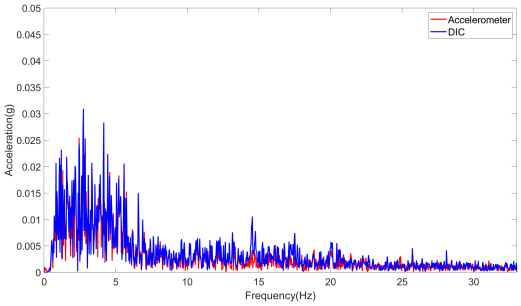

(j) Comparison of acceleration U direction at point D.

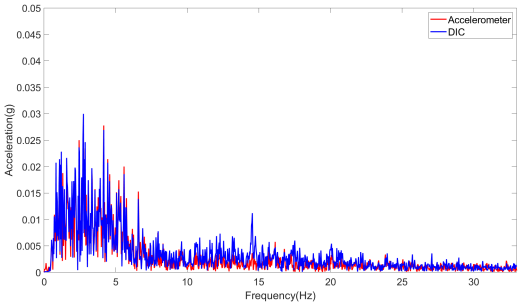

(k) Comparison of acceleration U direction at point E.

Figure 13. Frequency domain comparison between DIC measurements and accelerometer results.

As illustrated in **Figure 13**, the frequency domain results of acceleration show a strong correlation with the measurements obtained from the unidirectional accelerometers (A, B, C, D, and E) when compared to prediction points 2 and 3.

4.3. Full field of view results

The DIC method provides full-field acceleration and relative displacement results for the observation points. Note that the relative displacement is calculated by the difference between the calculation point on the graphite brick core and the relative speckle pattern on the fixture, as shown in **Figure 14**.

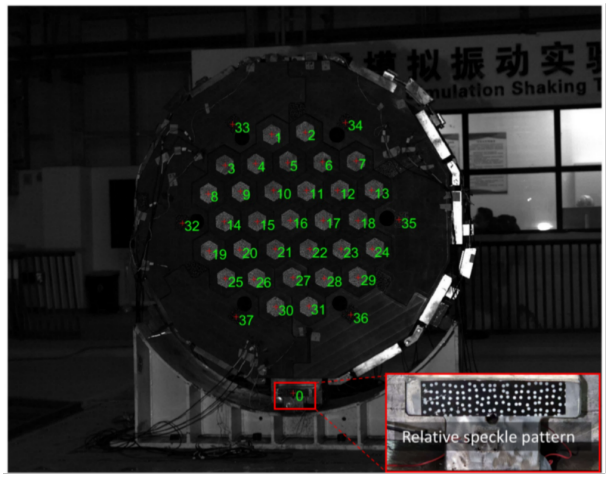

Figure 14. Calculation point number and reference speckle pattern.

A visual comparison of the maximum acceleration point and the relative displacement point is illustrated in **Figure 15**. The maximum acceleration of the core structure occurs at the top, where the relative displacement between the top and the

boundary is the greatest. The relative displacement in **Figure 15a** is the displacement relative to the bottom fixed point.

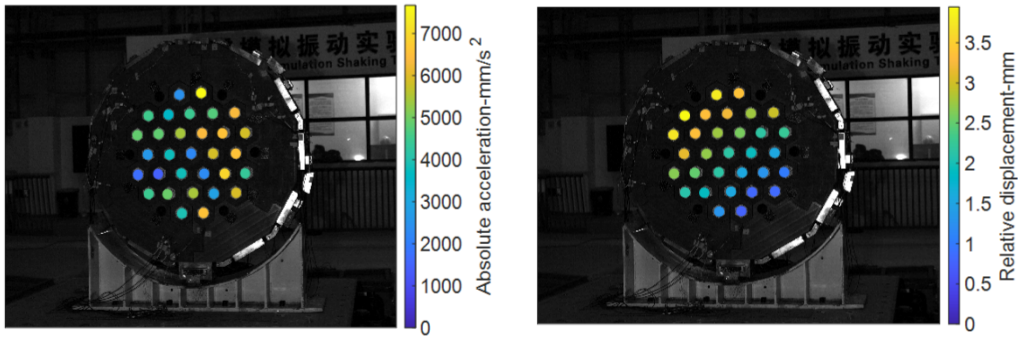

(a) Results of absolute acceleration. **(b)** Results of relative displacement.

Figure 15. Comparison of structural full-field results.

Since the gas-cooled micro-reactor features a horizontal layout, the control rods are inserted in a cantilever configuration. It is essential to meticulously manage the relationship between the control rod insertion holes and the control rods to prevent misalignment, which could hinder the rods' ability to drop under accidental operating conditions. There are six control rod insertion holes located in the outer reflective layer of the graphite core. To ensure the reactor can be safely and effectively shut down during accidental events, such as earthquakes, it is crucial to avoid significant interlayer dislocation of the control rod insertion holes. The control rod insertion holes are illustrated in **Figure 14**, with the holes marked by measurement points 32, 33, 34, 35, 36, and 37 representing the control rod insertion locations. The 0-point position serves as a fixed constraint point.

Using the DIC method, the coordinates of the control hole locations were calibrated, and their displacements relative to the fixed point 0 under seismic excitation are presented in **Figure 16**. This figure illustrates the relative displacements of the control holes within the core.

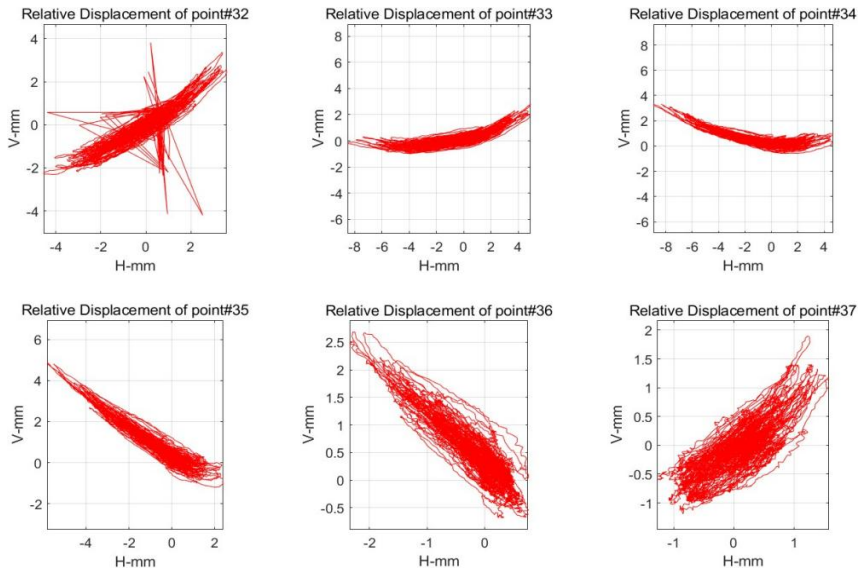

Figure 16. Relative displacement of the control rod insertion hole under seismic excitation [24].

The relative displacements of the top measurement points 32, 33, and 34 are

significant, and their displacements can be encompassed by a circle with a radius of 1 cm. In contrast, the relative displacements of the bottom circular hole are minimal. Therefore, in the design of the deflection or reserved space for the control rods, it is essential to allocate at least 1 cm or more of radial space to prevent contact between the control rods and the graphite bricks. It is advisable to reserve a gap of 2 cm or to consider the potential contact between the control rods and the aperture from a conservative perspective. Under the current earthquake intensity, after the seismic loads, no visible damage or wear was observed in the graphite structure, including visible cracks, chipped edges, or missing corners.

5. Discussion

From the measurement results, it can be observed that, in terms of phase, the results from the non-contact measurement system align closely with those obtained from the accelerometer. However, regarding amplitude, the acceleration amplitude recorded by the non-contact measurement system is significantly smaller than that of the accelerometer measurement. The relative error is calculated using Equation (2):

$$Relative\ Error = \frac{Accel_{DIC} - Accel_{Accelermeter}}{Accel_{Accelermeter}} \times 100\% \tag{2}$$

Figure 17 presents a histogram illustrating the distribution of relative errors. The majority of non-contact measurements fall within ±10% of the accelerometer measurements, which characterizes the stability and reliability of the data.

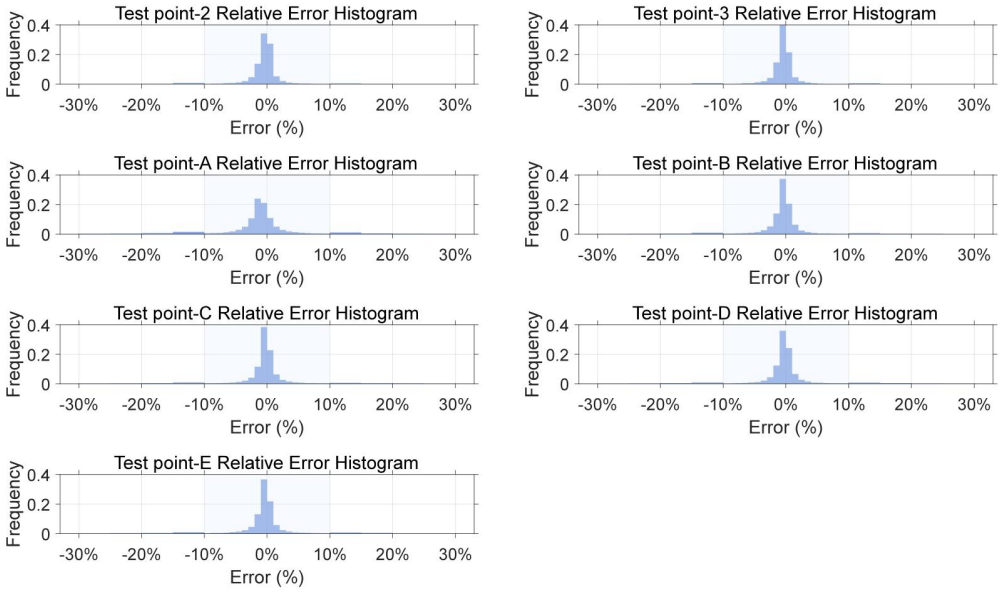

Figure 17. Histogram of relative error distribution of test points.

After removing significant outliers, the relative error-time variation curves of the non-contact measured acceleration and accelerometer acceleration were calculated, as shown in **Figure 18**.

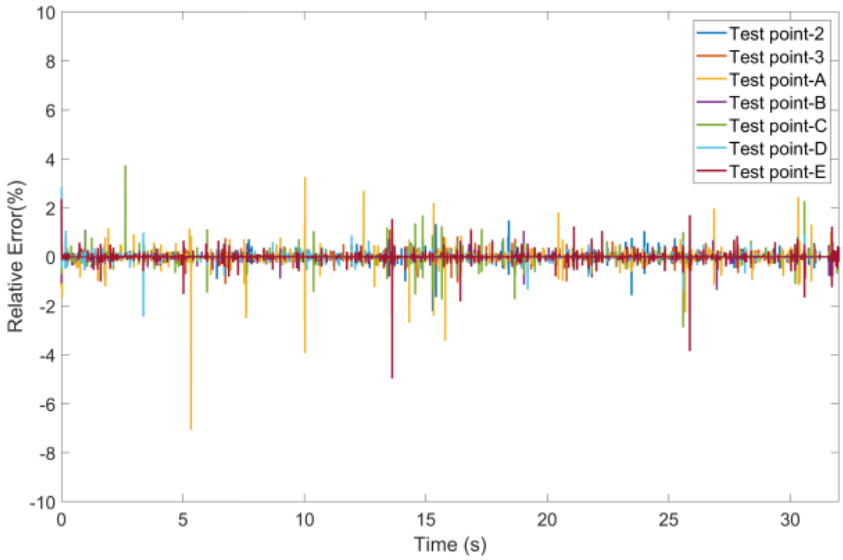

Figure 18. Non-contact measurement-accelerometer relative error variation curve.

This difference primarily arises from the following technical principles and systematic errors.

The DIC method requires numerical differentiation of the displacement data twice to derive the acceleration value; however, this process can amplify noise. The DIC calculates the average displacement over the region of interest (ROI), while the accelerometer measures the local response at a single point. In addition, due to installation errors, the installation direction of the accelerometer cannot be ideally horizontal or vertical. Therefore, the current results are acceptable, and the subsequent design process can be streamlined by incorporating a measured uncertainty factor. The DIC method does not interfere with the motion of lightweight or discrete structures (e.g., graphite blocks), avoiding mass-loading effects. DIC method can provide simultaneous displacement and strain data for the entire visible surface, capturing global deformation patterns and local interactions between components which can track numerous points (e.g., multiple graphite blocks and control rod holes) from a single setup, offering detailed kinematic information. While accelerometers provide direct, high-fidelity, and high-frequency recordings of acceleration, which is crucial for analyzing dynamic impacts and high-frequency vibrations. Accelerometers are excellent for capturing transient events and precise time-history data, essential for frequency and damping analysis which is well-established and reliable.

The study demonstrates the complementary nature of both techniques. Accelerometers are optimal for direct, high-frequency dynamic characterization at specific points, while DIC excels in providing non-contact, full-field displacement mapping of complex, discrete assemblies. Their integrated use, as shown in the paper, provides a more complete understanding of the structural seismic response.

6. Conclusion

In this study, vibration measurements of a discrete core structure were conducted, and the vibration of a graphite assembly was accelerated using both

non-contact measurements and accelerometers. The approximate accuracy range of the measurement results was initially determined through cantilever beam measurement tests. The reliability of the non-contact measurements was compared to the accelerometer results in terms of time and frequency domains, with the accelerometer data serving as a benchmark. For the first time, the DIC method was employed to measure the vibration response of graphite core structures. This paper presents a comparison and validation of the targeted measurement methods for bulk structures, and the control results indicate that:

Non-contact measurements can be employed to assess the vibrational characteristics of graphite discrete structures, avoiding excessive cable interference with the structure.

The 3D-DIC measurement results can accurately reflect the full field vibrational response of the graphite core structure.

The non-contact and acceleration measurements exhibit good phase agreement, with the maximum error between the two methods in amplitude remaining within 10%. This level of accuracy meets the requirements for engineering measurements.

The relative displacement of the control rod orifice under seismic loading is determined through seismic wave testing. This testing ensures that the control rod maintains a minimum clearance of more than 2 cm in the radial direction, preventing contact with the graphite blocks.

According to the measurements, the acceleration of the structure increases with height, and the acceleration of the graphite bricks in contact with the reflective layer is greater than that of the bricks located in the center.

The findings of this paper offer essential data to support the engineering safety design of gas-cooled microreactors and enhance the numerical model for future reference. Additionally, it serves as a valuable resource for the research and development of reactor types, such as molten salt reactors with a horizontally arranged graphite core structure.

Author contributions: Conceptualization, TL and ZZ; methodology, ZZ; software, TL; validation, TL and SZ; formal analysis, TL; investigation, TL; resources, ZZ; data curation, ZZ; writing—original draft preparation, TL; writing—review and editing, TL; visualization, TL. All authors have read and agreed to the published version of the manuscript.

Funding: This research was funded by China Nuclear Power Engineering Co., Ltd.(CNPE), grant number KY21090, and the APC was also funded by CNPE.

Institutional review board statement: Not applicable.

Informed consent statement: Not applicable.

Data availability statement: Data will be made available on request.

Conflict of interest: On behalf of all authors, the corresponding author states that there is no conflict of interest.

References

1. Shropshire D, Black G, Araújo K. Global market analysis of microreactors. Idaho National Laboratory; 2021. doi: 10.2172/1806274
2. Nuclear Energy Agency. Small modular reactors: challenges and opportunities. OECD/NEA; 2021. doi: 10.1787/18fbb76c-en
3. International Atomic Energy Agency. Advances in small modular reactor technology developments: A supplement to IAEA advanced reactors information system (ARIS). IAEA; 2020.
4. Lan T, Peng X, Sheng F, et al. Seismic modeling and simulation of the graphite core in gas-cooled micro-reactor. Nuclear Engineering and Design; 2025; 431: 113714.
5. Ahmed K, Stojko S. The non-linear seismic response of AGR core graphite brick slices: Correlation of experimental and analytical results. Earthquake Engineering and Structural Dynamics; 1987; 15(2): 159–188.
6. Ikushima T. SONATINA-2H: A Computer Program for Seismic Analysis of the Two-Dimensional Horizontal Slice HTGR Core. Japan Atomic Energy Research Institute; 1990.
7. Theymann W, Kemter F, Schmidt G. Seismic behavior of the core structure in a medium-sized HTR. In: Proceedings of the 10th International Conference on Structural Mechanics in Reactor Technology; 22–27 August 1989; Anaheim, CA, USA.
8. Sun L, Shi L, Wang H, et al. Seismic study on double-layer model of HTR graphite core structure. Atomic Energy Science and Technology; 2012; 46(S2): 839–844.
9. Lai S, Sun L, Shi L, et al. Seismic test and analysis on HTR-PM side-reflector structure similarity model. Atomic Energy Science and Technology; 2016; 50(4): 691–697.
10. Tian Q, Sun L, Wang H, et al. Seismic tests and analysis of HTR graphite single column model. Nuclear Power Engineering; 2012; 33(2): 42–46.
11. Wang H, Sun L, Wang H, et al. Experimental study on dynamic collision of nuclear graphite bricks. The International Conference on Computational & Experimental Engineering and Sciences; 2011; 17(1): 9–10.
12. Kemter F, Schmidt G. Seismic behaviour of the pebble bed in an HTR plant. In: Proceedings of the 8th International Conference on Structural Mechanics in Reactor Technology; 19–23 August 1985; Brussels, Belgium.
13. Kleine-Tebbe K A, Kemter F. Seismic behavior of the core cavern of a HTGR with pebble bed core. In: Proceedings of the IAEA IWGGCR Specialists' Meeting on Gas-Cooled Reactor Seismic Design Problems and Solutions; 30 August–1 September 1982; San Diego, CA, USA. pp. 119–132.
14. Ikushima T, Honma T, Ishizuka H. Seismic research on block-type HTGR core. Nuclear Engineering and Design; 1982; 71(2): 195–215.
15. Iyoku T, Inagaki Y, Shiozawa S, et al. Seismic study of high-temperature engineering test reactor core graphite structures. Nuclear Technology; 1992; 99(2): 158–168.
16. Ikushima T. Seismic Study on High Temperature Gas-Cooled Reactor Core. Japan Atomic Energy Research Institute; 1991.
17. Ikushima T, Honma T. Seismic response of high temperature gas-cooled reactor core with block-type fuel (II): Three-dimensional vibration characteristics of stacked block column. Journal of Nuclear Science and Technology; 1980; 17(9): 655–667.
18. Ikushima T, Honma T. Seismic response of high temperature gas-cooled reactor core with block-type fuel (III): Vibration experiment of two-dimensional vertical slice core model. Journal of Nuclear Science and Technology; 1981; 18(7): 514–524.
19. Olsen BE, Neylan AJ, Gorholt W. Seismic test on a one-fifth scale HTGR core model. Nuclear Engineering and Design; 1976; 36(3): 355–365.
20. Ni ZS, Sun LB, Wu XX. Research on the application of wireless acceleration sensors in graphite core structure seismic experiment. Nuclear Power Engineering; 2014; 35(1): 170–173.
21. Voyagaki E, Kloukinas P, Dietz M, et al. Earthquake response of a multiblock nuclear reactor graphite core: Experimental model vs simulations. Earthquake Engineering and Structural Dynamics; 2018; 47(13): 2601–2626.
22. Dihoru L, Oddbjornsson O, Kloukinas P, et al. The development of a physical model of an advanced gas cooled reactor core: Outline of the feasibility study. Nuclear Engineering and Design; 2017; 323: 269–279.
23. Gokce T, White RE, Crewe AJ, et al. Seismic response prediction using intensity measures: Graphite nuclear reactor core model case study. Earthquake Spectra; 2023; 39(4): 1992–2018.

24. Lan T, Long B, Peng X, et al. A study on the seismic test of a planar model of the gas-cooled microreactor. Nuclear Engineering and Technology; 2025; 58(2): 103984.
25. Parsi SS, Whittaker AS, Sivaselvan MV, et al. Experimental investigations into the rocking response of graphite-block assemblies in a HTGR core under horizontal earthquake shaking. Nuclear Engineering and Design; 2025; 443: 114300.
26. Khanahmadi M. A cutting-edge framework for damage-sensitive feature extraction leveraging modal dynamic flexibility in signal processing-driven structural health monitoring. Thin-Walled Structures; 2025; 216(A): 113617.
27. Khanahmadi M, Mirzaei B, Amiri GG, et al. A mode shape sensitivity-based wavelet feature extraction method for interface debonding detection in concrete-filled steel tubes. Measurement Science and Technology; 2024; 36(1): 016137.
28. Lan T, Feng T, Huang Z, et al. A preliminary study on seismic analysis of graphite cores for gas-cooled microreactor. Nuclear Techniques; 2025; 48(10): 100003.